ISSN 0031-918X, The Physics of Metals and Metallography, 2016, Vol. 117, No. 3, pp. 238–245. © Pleiades Publishing, Ltd., 2016.
Original Russian Text © A.E. Galashev, 2016, published in Fizika Metallov i Metallovedenie, 2016, Vol. 117, No. 3, pp. 250–257.

STRUCTURE, PHASE TRANSFORMATIONS, AND DIFFUSION

Molecular-Dynamic Simulation of the Removal of Mercury from Graphene via Bombardment with Xenon Clusters

A. E. Galashev

Institute of High-Temperature Electrochemistry, Ural Branch, Russian Academy of Science, ul. S. Kovalevskoi 22, Ekaterinburg, 620137 Russia

e-mail: alexander-galashev@yandex.ru

Received January 26, 2015; in final form, September 22, 2015

Abstract—The method of molecular dynamics has been used to study the removal of mercury from graphene by irradiating the target using a beam of Xe_{13} clusters with energies of 5–30 eV at angles of incidence of 0°, 45°, and 60°. The edges of the graphene sheet were hydrogenated. The complete removal of mercury from graphene was achieved at the angles of incidence of clusters equal to 45° and 60° with the energies of the beam $E_{Xe} \geq 15$ and 10 eV, respectively. A substantial part of the film was separated from graphene in the form of a droplet. The form of the distributions of stresses in the graphene sheet indicates the absence of enhancement of the stressed state in the course of the bombardment. The bombardment at the angle of incidence of clusters equal to 45° leads to the lowest roughness of graphene. As a result of the bombardments in the above ranges of energies and angles of cluster incidence, the hydrogenated edges of the graphene sheet did not suffer significant damage.

Keywords: graphene, clusters of xenon atoms, stresses, film, mercury

DOI: 10.1134/S0031918X16030042

INTRODUCTION

Mercury is the only metal among the most abundant ones that remains liquid at room temperature. The study of the adsorption of mercury on activated carbon was, as a rule, carried out experimentally. There is a limited number of theoretical studies concerning this theme. Steckel [1] investigated the interaction between elemental mercury and a single benzene ring in order to explain the mechanism through which elemental mercury is bound with carbon. Padak et al. [2] investigated the effect of different surface functional groups and halogens present on the surface of activated carbon on the adsorption of elemental mercury. It has been established that the addition of halogen atoms intensifieds the adsorption of mercury. In [3], Padak and Wilcox have demonstrated a thermodynamic approach to the examination of the mechanism of binding of mercury and its capture in the form of HgCl and $HgCl_2$ on the surface of activated carbon. The energies of different possible surface complexes have been determined. In the presence of chlorine, the mercury atoms strongly cohere to the surface. In the case of dissociative adsorption, Hg can undergo desorption, while HgCl remains on the surface. The compound $HgCl_2$ was not found on the stable carbon surface [4]. Understanding of the mechanism of the adsorption of mercury on activated carbon is important for the development of efficient technologies for capturing mercury.

Mercury is one of the most toxic heavy metals, and its presence is due to a combination of natural processes (volcanic activity, erosion of the mercury-containing sediments) and anthropogenic activity (extraction of minerals, pollution from the leather-dressing production and metallization of objects). Adsorption is considered to be one of the most efficient and economical methods of removing mercury from wastewater and air. Recently, graphene membranes began to be used for capturing supersmall amounts of substances [5]. The repeated application of graphene in the filters requires its nondestructive cleaning from the adsorbates. The removal of metals from graphene can be produced by its irradiation by a beam of rare-gas clusters [6–11]. The use of cluster beams for the surface cleaning is more efficient than the application of ion beams for this purpose. In this case, the energy of a cluster grows in proportion to the number of atoms in the cluster at the same velocity of the projectile and, thus, it is possible to avoid large optical aberrations in the focusing systems. Bombardment using cluster projectiles proves to be much more sparing in comparison with the ionic bombardment, since a cluster projectile cannot penetrate the target so deeply as an atomic analog can. In the prospect, the application of cluster beams will make it possible to create a number of fundamentally new technologies of the surface cleaning and to develop a new generation of ionic sources.

This work is aimed at studying the possibility of removing adsorbed mercury from graphene by means of bombardment by xenon clusters.

MOLECULAR-DYNAMIC MODEL

The interatomic interactions in graphene are represented by the many-body Tersoff potential [12]. The energy of pairwise interaction of atoms i and j taking into account the influence of other atoms (multiparticle effects) is written as

$$V_{ij} = f_C(r_{ij})\left[A\exp(-\lambda^{(1)}r_{ij}) - Bb_{ij}\exp(-\lambda^{(2)}r_{ij})\right], \quad (1)$$

$$f_C(r_{ij}) = \begin{cases} 1, \\ \frac{1}{2} + \frac{1}{2}\cos\left[\pi\left(r_{ij} - R^{(1)}\right)\Big/\left(R^{(2)} - R^{(1)}\right)\right], \\ 0 \end{cases} \quad (2)$$

$$\begin{matrix} r_{ij} < R^{(1)} \\ R^{(1)} < r_{ij} < R^{(2)}. \\ r_{ij} > R^{(2)} \end{matrix}$$

Here, r_{ij} is the spacing between the atoms i and j and the parameters A and B are the energy characteristics of the repulsion and attraction. The many-body parameter of the bond order b_{ij} describes how the binding energy (attractive part V_{ij} of the bond) is formed during a local atomic arrangement due to the presence of other neighboring atoms. The function f_C decreases from 1 to 0 in the region of $R^{(1)} \le r_{ij} \le R^{(2)}$. The parameters $R^{(1)}$ and $R^{(2)}$ were selected so as to include into the consideration only nearest neighbors. The potential energy is a many-body function of the positions of atoms i, j, and k and is determined by the parameters

$$b_{ij} = (1 + \beta^n \xi_{ij}^{n_i})^{-1/(2n)}, \quad (3)$$

$$\xi_{ij} = \sum_{k \neq i,j} f_C(r_{ij})g(\theta_{ijk}), \quad (4)$$

$$g(\theta_{ijk}) = 1 + \frac{c^2}{d^2} - \frac{c^2}{\left[d^2 + (h - \cos\theta_{ijk})^2\right]}, \quad (5)$$

where the parameters n, n_i, and β set the binding force depending on the environment. The effective coordination number ξ_{ij} determines the average number of nearest neighbors with taking into account not only the distances between them, but also the bond angles θ_{ijk}. The summing up in expression (4) is conducted over all k first-order neighbors not equal to i and j. These neighbors are selected for each i–j pair and are defined at each time moment; $g(\theta_{ijk})$ is the function of the angle between $\mathbf{r}_{ij}$ and $\mathbf{r}_{ik}$, where $\mathbf{r}_{ij}$ is the vector drawn from the point of the location of the atom i to the point where the atom j is located. The parameter d assigns the width of the sharp maximum in the $g(\theta_{ijk})$ angular dependence, the parameter c assigns the height of this peak, and the function $g(\theta_{ijk})$ has a minimum at $h = \cos\theta$. All parameters of the potential were selected so that to match the theoretical and experimental data (energy of cohesion, lattice parameters, bulk moduli) for a real and hypothetical graphite and diamond.

Because of the insufficiently precise determination of the force characteristics that control the C–C bonds, the Tersoff potential does not have a barrier to the rotation about the single bond. The inadequacy of the semiempirical Tersoff potential is revealed when studying the dynamic properties of graphite; it manifests itself in the rotation of the entire fragment to be simulated and can be corrected by adding a torsion-like term [13]. The parameters of this potential were refined via fitting to the observed properties (standard deviations for the vibration frequencies) of graphite and diamond. The new analytical form of the potential of local torsion is given in [14]. The use in this work of weighting functions for the bond orders ensures a smooth removal of the energy of torsion connected with the dihedral angle upon any sequential break of bonds [14]. The distance $R^{(2)}$ of the covalent binding in the original Tersoff potential was limited to the value of 0.21 nm. The simulation of graphene with this potential led not only to an uncontrollable rotation, but also to the cracking of the graphene sheet [15, 16]. Therefore, we increased the value of r_b to 0.23 nm and also included an additional weak attraction at $r > 0.23$ nm assigned by the Lennard-Jones (LD) potential with the parameters used in [14].

The pair potential that was utilized for the description of Hg–Hg interactions was proposed in [17] in the following form:

$$V_{\mathrm{Sch}}(r) = \sum_{j=3}^{9} a_{2j}^* r^{-2j}. \quad (6)$$

The authors of [17] corrected the original Schwerdtfeger (SCH) potential [18] for mercury dimer by scaling distances using the coefficient $\lambda = 1.167$. The parameters a_{2j}^* represented in [17] correspond to the density of liquid Hg at $T = 300$ K.

The Hg–C and Xe–Xe interactions were assigned by a Lennard-Jones potential with the parameters established in [19, 20]. The interaction between Xe atoms and the atoms of the target (Hg and C) was

assigned by a purely repulsive Ziegler–Biersack–Littmark (ZBL) potential as follows [21]:

$$\Phi = Z_i Z_j \frac{e^2}{r}\left\{0.1818\exp\left(-3.2\frac{r}{a}\right) + 0.5099\exp\left(-0.9423\frac{r}{a}\right) + 0.2802\exp\left(-0.4029\frac{r}{a}\right) + 0.02817\exp\left(-0.2016\frac{r}{a}\right)\right\}, \quad (7)$$

where Z_i and Z_j are the atomic numbers of the atoms i and j; e is the elementary electric charge; r is the interatomic distance; and the parameter a is determined by the expression

$$a = 0.8854a_0\left(Z_i^{0.23} + Z_j^{0.23}\right)^{-1}. \quad (8)$$

where a_0 is the Bohr radius. We disregard the weak attraction between the atoms of Xe and Hg and also between Xe and C, since the primary purpose of this investigation is the examination of the transfer of energy and momentum rather than of the chemical bonding [22].

Hydrogenation was employed to strengthen the graphene edges. The CH groups that were formed at the edges of the sheet were simulated according to the monatomic scheme [23]. The C–CH and CH–CH interactions were represented via an LD potential [23]. The connection of H atoms to the edges of a graphene sheet does not change the interatomic distances and does not create a roughness of its surface.

A film of mercury on graphene was formed in a separate molecular-dynamic (MD) calculation in two stages. At the first stage, the Hg atoms were placed above the centers of nonadjacent cells of graphene in such a way that the interatomic distance between Hg and C atoms be equal to 2.30 Å, calculated according to the density-functional method [24]. On top of this loose film consisting of 49 mercury atoms, 51 additional Hg atoms were deposited randomly. Then, the system, which consists of 100 atoms of Hg and 406 atoms of C, was brought to equilibrium in the MD calculation with a duration of 1 million time steps ($\Delta t = 0.2$ fs). For the numerical solution of the equations of motion, the Verlet algorithm was used [25]. The thus-obtained target was then bombarded with icosahedral Xe_{13} clusters. Five starting points for the positioning of the centers of Xe_{13} clusters were located uniformly along a line parallel to the oy axis (the armchair direction). This line was placed either along the left-hand edge of the graphene sheet (upon the vertical bombardment) or with an additional displacement to the left from it (upon the inclined bombardment), and was lifted to a height of 1.5 nm in the direction of the oz axis. The interval equal to the length of the graphene sheet in the direction of the ox axis (the zigzag direction) was divided into five equal sections with a length $L_i = L_x/5$. At the beginning of every subsequent cycle of cluster impacts, the line of the starting points of the Xe_{13} clusters was horizontally moved forward by a distance L_i. As a result, the surface of the film approximated by the plane was covered with 25 evenly distributed points at which the cluster impacts were aimed. Each series included 5 cycles, or 25 impacts. At the starting point, all atoms of the Xe_{13} cluster were given the same velocity in the direction of bombardment. The clusters were in turn sent toward the target. The lifetime (determined by the sum of the time of flight and time of interaction with the target) of each cluster was limited to 8 ps. After this time, the Xe atoms of the destroyed cluster were excluded from the consideration and a new Xe_{13} cluster began moving from another initial point. The cycle of bombardment by five clusters took 40 ps, while the series of five cycles took 0.2 ns and the entire time of bombardment (five series) took 1 ns. The clusters used for bombardments had kinetic energies of 5, 10, 15, 20, and 30 eV; the angles of incidence were 0°, 45°, and 60°.

The impact of a cluster on the surface was accompanied by heating the system. The moderate removal of the heat released from the system was performed according to the Berendsen scheme with the coupling time constant $\tau_c = 4$ fs [26]. The forced reduction in the temperature was conducted via the scaling of velocities v at each time step as follows:

$$v \to \lambda v, \quad \lambda = \left[1 + \frac{\Delta t}{\tau_c}\left(\frac{T_0}{T} - 1\right)\right]^{1/2}, \quad (9)$$

where λ is the scaling factor, T_0 is the assigned temperature (300 K), and T is the current temperature.

The density profile of the metallic film was calculated as follows:

$$\rho(z) = \frac{n(z)\sigma_{Hg}^3}{\Delta h S_{xy} N_s}, \quad (10)$$

where $n(z)$ is the number of Hg atoms in the layer parallel to the plane of the grapheme, σ_{Hg} is the effective diameter of the Hg atom, Δh is the width of the layer, S_{xy} is the area of the graphene surface, and N_z is the number of tests.

The self-diffusion coefficient was defined through the mean square of the displacement $\left\langle\left[\Delta\mathbf{r}(t)\right]^2\right\rangle$ of the system consisting of N atoms of Hg as follows:

$$D = \frac{1}{2\Gamma}\lim_{\tau\to\infty}\frac{1}{\tau}\left\langle\left[\Delta\mathbf{r}(t)\right]^2\right\rangle_p. \quad (11)$$

Here, $\Gamma = 3$ is the dimensionality of space; $\langle\ldots\rangle$ means averaging over p, where p is the number of time intervals (with the initial time t_0) for the determination of $\left[\Delta\mathbf{r}(t)\right]^2 = \frac{1}{N}\sum_{j=1}^{N}\left[\mathbf{r}_j(t) - \mathbf{r}_j(t_0)\right]^2$, and $\mathbf{r}_j$ is the radius vector of the atom j. Averaging is performed over five

time dependences, each calculated in an interval τ = 200 ps.

To calculate stresses that appear in graphene, the graphene sheet was divided into surface elements. The stresses $\sigma_{u\alpha}(l)$ that appear under the action of the forces of direction α (= x, y, z) are calculated on each element with the order number l that has the orientation u. In these calculations, products of the projections of the velocities of atoms and the projections of the forces that act on the lth element from the other atoms with the fulfillment of corresponding conditions are used as follows [27, 28]:

$$\sigma_{u\alpha}(l) = \left\langle \sum_{i}^{k} \frac{1}{\Omega}\left(m v_u^i v_\alpha^i\right)\right\rangle + \frac{1}{S_l}\left\langle \sum_{i}^{k} \sum_{j\neq i}^{(u_i\le u, u_j\ge u)} \left(f_{ij}^{\alpha}\right)\right\rangle. \quad (12)$$

Here, k is the number of atoms on the element l, Ω is the volume per atom, m is the mass of an atom, v_α^i is the α projection of the velocity of atom i, and S_l is the area of the element l. The conditions for summation over j in the last sum in expression (12) are given in the lower and upper indices of the sum, the force that appears upon the interaction of atoms i and j goes through the lth element, and u_i is the current coordinate of the atom i (u can take values x, y, z). In the case when u=z, u represents the average level (height) of atoms C in graphene.

The graphene sheet had dimensions of 3.4 × 2.8 nm and contained 406 atoms. Each element l separated on this sheet and elongated along the axis oy (perpendicular to the zigzag direction of graphene) contained 14 C atoms and had an area of 0.68 nm^2. Specifically, this layout corresponds to the data shown in Fig. 4. The total stresses that act in the plane of graphene were determined by summing the corresponding elementary stresses as follows:

$$\sigma_{u\alpha} = \sum_{l=1}^{N_l} \sigma_{u\alpha}(l), \quad (13)$$

where N_l is the number of surface elements.

The roughness of the surface (or the arithmetic mean deviation of the profile) was calculated as

$$R_a = \frac{1}{N_g}\sum_{i=1}^{N_g} |z_i - \overline{z}|, \quad (14)$$

where N_g is the number of sites (atoms) on the surface of the graphene sheet, z_i is the level of atom i, $\overline{z}$ is the level of the graphene surface, and the levels z_i and $\overline{z}$ are determined at the same time moment.

The total energy of a free one-sheeted graphene obtained at T = 300 K is equal to –7.02 eV, which is in agreement with the quantum-mechanical calculation (–6.98 eV) [29]. The value of the isochoric heat capacity of liquid mercury at this temperature (28.4 J/(mol K) calculated in the MD model agrees with the experimental value of 26.9 J/(mol K).

RESULTS OF CALCULATIONS

At a temperature of 300 K, mercury is in the liquid state (melting point T_m = 234 K). If the attraction forces between the Hg atoms exceed the forces of cohesion of the mercury film with graphene, the film contracts into a droplet. In order to investigate the opportunity to roll the film into the droplet, we carried out an MD calculation of an Hg film on graphene at T = 300 K using 10 million time steps in the absence of cluster bombardment. A drop of mercury on the graphene sheet close to a spherical shape was obtained as a result of this calculation. In this case, a substantial part of the lower surface of the drop that is in contact with graphene was flat. Thus, the film of mercury that was simulated based on the Schwerdtfeger interaction potential has a tendency to roll into a drop. The cluster bombardment using 125 impacts with an angle of incidence of 0° did not lead to any significant removal of mercury from graphene at all energies of Xe_{13} clusters in the range of 5–30 eV. As a rule, more than half of the Hg atoms after the completion of the bombardment were bound with graphene, as before. The bombardment at the angle of incidence equal to 45° was considerably more successful. In this case, beginning with the energy of beam equal to 15 eV, graphene was almost completely cleaned of mercury. Only single atoms could remain connected with the graphene sheet; moreover, the majority of these atoms were retained at the edges of the sheet. The remaining atoms of Hg were scattered far beyond the limits of the graphene sheet predominantly in two directions (in the horizontal direction at a sharp angle to the axis ox, and upward). As a rule, the Hg atoms were knocked out from the film one by one and less frequently in the form of dimers and trimers. However, at the energies of the cluster beam $E_{Xe} \ge 15$ eV there was always separated also a drop of mercury from graphene. An increase in the angle of incidence of the Xe_{13} clusters to 60° led to the removal of mercury from graphene at the energy of the beam of 10 eV (Fig. 1). A subsequent increase in the energy of the cluster beam at $\theta = 60°$ did not give a desired result: graphene was not cleaned of mercury.

The vertical profiles of the mercury density reflect the displacement of the atoms of metal predominantly upward as a result of the cluster bombardment of the target at the angle of incidence of clusters equal to $\theta = 0°$ (Fig. 2). The maximum of the density profile is consecutively displaced upward with increasing the energy of the bombarding clusters. A delay in this motion is observed only at E_{Xe} = 15 eV, where the position of the density maximum deflected slightly to the reverse side in comparison with the position for the profile at E_{Xe} = 10 eV. However, already at E_{Xe} = 20 eV,

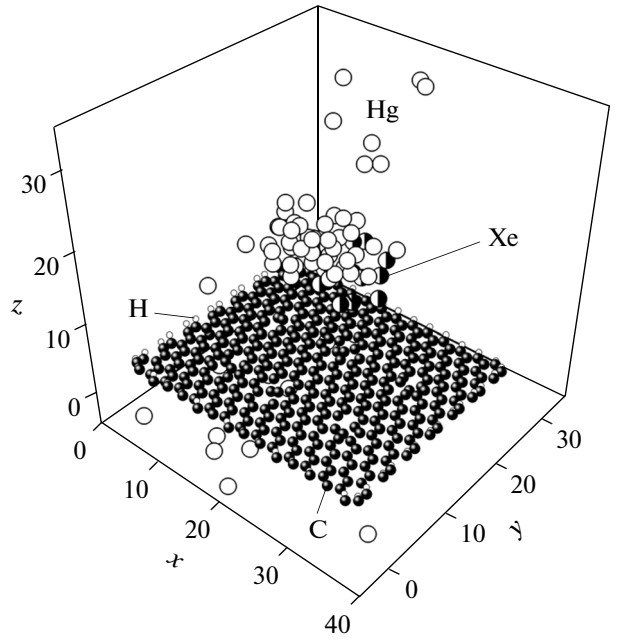

Fig. 1. Configuration of a system consisting of a mercury film on a partially hydrogenated imperfect graphene sheet after bombardment by a beam of Xe_{13} clusters at the angle of incidence of 60° and the energy equal to 10 eV. The coordinates of atoms are given in angstroms.

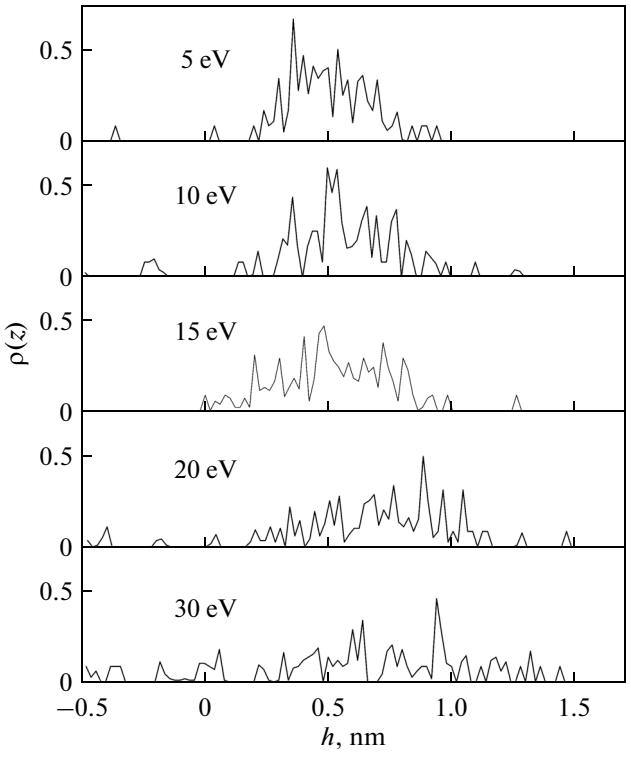

Fig. 2. Vertical profiles of the density of liquid mercury on graphene. Numbers (eV) indicate the energies of the falling clusters.

the position of the maximum density substantially increased in height and continued increasing at E_{Xe} = 30 eV. The density profiles at $E_{Xe} \geq 20$ eV increase their vertical extents in both directions (upward and downward).

With an increase in the angle of incidence of the xenon clusters, there occurs an increase in the self-diffusion coefficient of mercury atoms; especially, this is noticeable on going from the angle θ = 45° to the angle of 60°. The lowest value of the self-diffusion coefficient of Hg atoms is observed upon the vertical bombardment with the energy of Xe_{13} clusters equal to 5 eV (Fig. 3). At energies $E_{Xe} \geq 10$ eV and at an angle of incidence θ = 0°, there is a very weak dependence of the self-diffusion coefficient on the energy of the falling clusters. A similar weak dependence is manifested in the entire range of cluster energies at the angle of incidence θ = 45°. At the angle θ = 60°, the $D(E_{Xe})$ function has a deep minimum at 15 eV. The origin of this minimum is most likely connected with the fact that the bombardment with precisely such energy of clusters provides the most rapid rolling of the mercury film into a drop, from which the Hg atoms can be kicked out only with difficulty. Except for this specific feature, no significant changes in the behavior of the coefficient of self-diffusion is observed upon the variations in the energy E_{Xe} with an angle of incidence θ = 60°. The weak change in the $D(E_{Xe})$ function indicates the effective removal of heat that is separated upon the impacts using the Berendsen thermostat. In other words, the energy is not accumulated in the system in the course of the bombardment.

The $\sigma_{\alpha\beta}(E_{Xe})$ dependences of the stresses in the plane of graphene caused by horizontal (Figs. 4a, 4b) and vertical (Fig. 4c) forces exhibit a complex behavior, which is different for different angles of incidence. As a rule, the stresses σ_{zz} created by vertical forces are

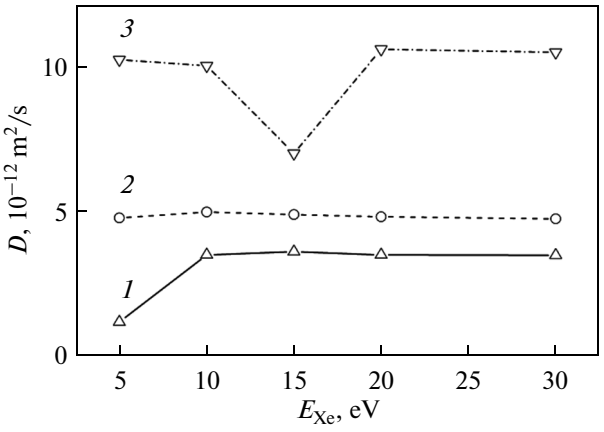

Fig. 3. Self-diffusion coefficients of Hg atoms calculated for the cases of bombardment of the target at the angles of incidence (*1*) 0°, (*2*) 45°, and (*3*) 60° depending on the energies of the cluster beam E_{Xe}.

noticeably higher than the stresses σ_{zx} and σ_{zy} that appear due to the action of horizontal forces. At cluster energies E_{Xe} that lead to the detachment of the majority of Hg atoms from graphene, the stress σ_{zz} has relatively low values. Recall that this occurs at energies $E_{Xe} \geq 15$ eV at an angle of incidence of 45° and at $E_{Xe} = 10$ eV at the angle $\theta = 60°$.

The roughness R_a of graphene increases continuously in the course of cluster bombardment. The inset in Fig. 5 gives a representation of the variation of the function $R_a(t)$ in time in the case of bombardment with an energy of Xe_{13} clusters equal to 15 eV at the angle of incidence of 0°. The bombardment has a significant effect on the roughness of graphene. The magnitude of R_a increases by 20–40%, even as a result of the bombardment with the energy of clusters equal to only 5 eV; the effect is strongest at an angle of incidence of 60°. The form of functions obtained at different values of the energy of the Xe clusters is shown in Fig. 5. It can be seen that the bombardment at an angle of $\theta = 45°$ leads to the lowest values of R_a. Thus, after this bombardment at an energy of the beam equal to 30 eV, the value of R_a proves to be below the appropriate characteristics that correspond to the angles of incidence of 0° and 60° by 9.6% and 11.8%, respectively.

DISCUSSION OF RESULTS

It is of interest to compare the results of the study of the removal of films of copper and lead by the bombardment with clusters of rare gases with the present investigation of the purification of graphene from mercury. First of all, the different mechanisms of the detachment of these heavy metals from graphene during the irradiation of the target by a cluster beam should be noted. In the case of the bombardment of the copper film with Ar_{13} clusters, separate Cu atoms are knocked out [6–11]. No regime of bombardment led to the separation of fairly large fragments of the Cu film from graphene. When the lead film is bombarded, separate atoms are also knocked out, but the prevailing mechanism of the removal of the metal form graphene is the separation of islands of a Pb film from the substrate [30]. Only when detached away from graphene, the island experiences a transformation from a two-dimensional to a three-dimensional structure; mercury is separated from graphene in a different way. The unique behavior of mercury is due to its liquid state and the poor wetting of graphene; as a result, the Hg film has a tendency to roll into a drop. For this reason, both separate atoms and droplets of significant size are separated from graphene in the course of bombardment. Let us emphasize that it is precisely a drop that is torn off, rather than an island with a two-dimensional morphology. There are several other differences in the processes of the removal of the film of heavy

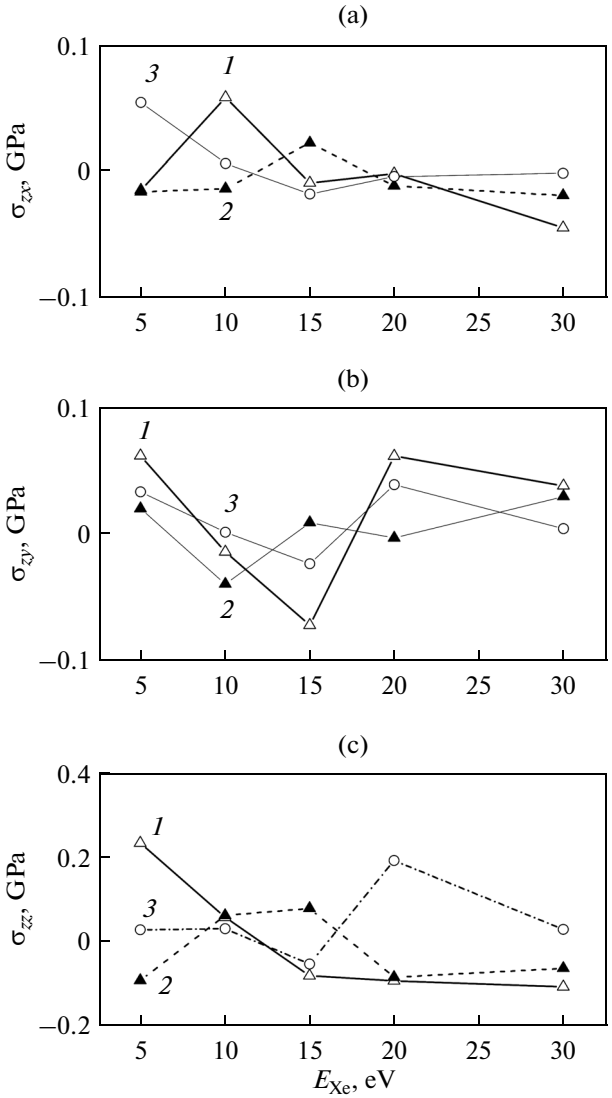

Fig. 4. Components of the stress tensor in graphene ((a) σ_{zx}, (b) σ_{zy}, (c) σ_{zz}) obtained for the cases of the bombardment of targets at the angles of incidence (*1*) 0°, (*2*) 45°, and (*3*) 60° depending on the energies of the cluster beam E_{Xe}.

metals from graphene. Thus, the film of copper is not completely removed from graphene, even at an energy of the beam equal to 30 eV at angles of incidence of 0° and 60° [6], and the most efficient method is removal using cluster bombardment at an angle $\theta = 45°$. In the case of lead, the most efficient procedure can be considered to be irradiation by a cluster beam at the angles of incidence of 0° and 60°. In this case, graphene was completely cleaned of metal at energies of the beam equal to 10 and 15 eV. The complete cleaning was also achieved at an angle $\theta = 45°$, but the energy of the cluster beam required in this case was equal to 20 eV. The greatest effect from the bombardment of the mer-

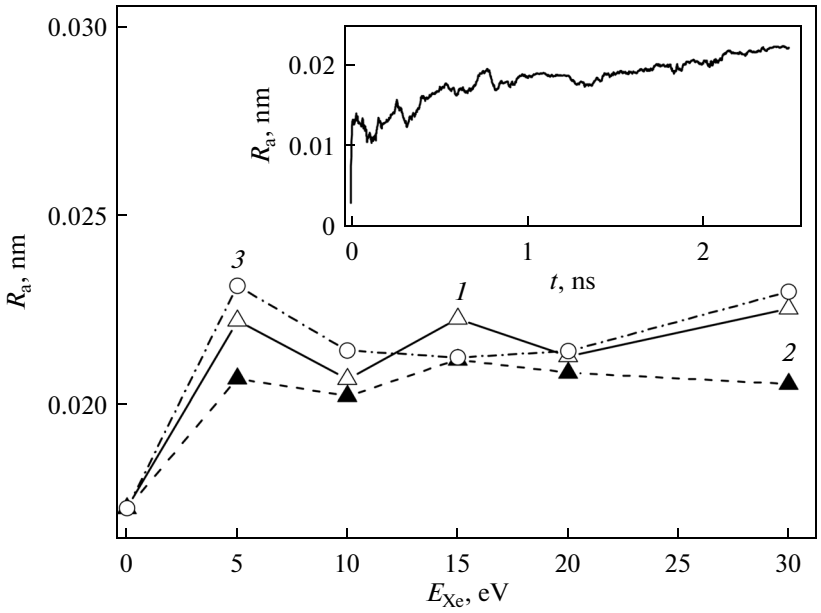

Fig. 5. Roughness of graphene obtained as a result of the bombardments of the target at the angles of incidence (*1*) 0°, (*2*) 45°, and (*3*) 60° at the energies of the cluster beam E_{Xe}. Inset shows the change in the roughness of graphene in the course of the bombardment of the target by Xe_{13} clusters at the angle of incidence equal to 0° and at an energy of the cluster beam of 15 eV.

cury-on-graphene target is obtained at an angle of incidence equal to 45°. At this angle of incidence, graphene is cleaned of Hg at all energies $E_{Xe} \geq 15$ eV. A less stable cleaning effect was achieved at an angle of incidence of 60°. In the case of an angle of incidence equal to 0°, no significant removal of mercury from graphene occurs in the range of energies of the beam equal to 5–30 eV. Thus, the removal of different heavy metals requires different conditions for bombardment and occurs via different mechanisms.

To check the correctness of the results, we also conducted calculations with another pair potential for mercury and another potential that describes the mercury–graphene interaction. The Hg–Hg interactions were determined based on applying the potential proposed by Silver and Goldman (SG potential) with the parameters given in [31]. Here, we obtained results close to those where the SCH potential served as the potential function for mercury. In the calculations that applied the SG potential, upon bombardment, the Hg film was more rapidly transformed into the drop and was separated from graphene. The complete removal of mercury from graphene was only achieved at an angle of incidence equal to 45° at $E_{Xe} \geq 15$ eV. When using a Morse potential with the parameters given in [32] for the representation of Hg–C interactions, mercury upon the bombardment was separated from graphene more difficult, and the complete cleaning at the angle $\theta = 45°$ was achieved at the energies $E_{Xe} \geq 20$ eV.

CONCLUSIONS

The behavior of a system of mercury-on-partially-hydrogenated-graphene has been investigated under irradiation by a beam of Xe_{13} clusters with energies of 5–30 eV at the angles of incidence equal to 0°, 45°, and 60°. Over a wide range of energies ($E_{Xe} \geq 15$ eV), the almost complete removal of mercury from graphene was only achieved at an angle of incidence of 45°. The film of mercury, which has a tendency to become rolled up into a drop, is separated from graphene in the form of single atoms, dimers, trimers, and spherical droplets. In the course of the bombardment, mercury exhibits a weak cohesion with graphene. With an increase in the energy of the falling clusters from 5 to 30 eV, the $h(z)$ profile evolves in a complex way, demonstrating the formation of a drop of mercury on graphene, as well as the formation of a vapor of Hg monomers. The smallest change in the components of the mobility of Hg atoms upon the variation of the energy of the cluster beam occurs at the angle of incidence equal to 45°. At the energies of the cluster beam under consideration, the stresses in the plane of graphene caused by the vertical forces noticeably exceed the stresses created by the horizontally directed forces, regardless of the angle of incidence. The roughness of graphene increases noticeably in the course of cluster bombardment. The lowest roughness is demonstrated by graphene subjected to irradiation with the beam of clusters with an angle of incidence equal to 45°. The hydrogenated edges of graphene do not suffer notice-

able damages at all the energies investigated and at all the angles of incidence of the bombarding clusters.

ACKNOWLEDGMENTS

This work was performed within the framework of a state task of the FANO of the Russian Federation (theme "Electrode Reactions of Electrochemical Technologies of Refining and Obtaining Metals and Their Compounds in Molten Salts," no. 0395-2014-0004) and was supported in part by the Russian Foundation for Basic Research (project no. 13-08-00273).

REFERENCES

1. J. A. Steckel, "Ab initio modelling of neutral and cationic Hg–benzene complexes," Chem. Phys. Lett. **409**, 322–330 (2005).
2. B. Padak, M. Brunetti, A. Lewis, and J. Wilcox, "Mercury binding on activated carbon," Environ. Prog. **25**, 319–326 (2006).
3. B. Padak and J. Wilcox, "Understanding mercury binding on activated carbon," Carbon **47**, 2855–2864 (2007).
4. F. E. Huggins, G. P. Huffman, G. E. Dunham, and C. L. Senior, "XAFS examination of mercury sorption on three activated carbons," Energy Fuels **13**, 114–121 (1999).
5. Y. Cao and X. Li, "Adsorption of graphene for the removal of inorganic pollutants in water purification: A review," Adsorption, **20**, 713–727 (2014).
6. A. E. Galashev and V. A. Polukhin, "Removal of copper from graphene by bombardment with argon clusters: Computer experiment," Phys. Met. Metallogr. **115**, 697–704 (2014).
7. A. E. Galashev and A. A. Galasheva, "Molecular dynamics simulation of copper removal from graphene by bombardment with argon clusters," High Energy Chem. **48**, 112–116 (2014).
8. A. E. Galashev, "Computer simulation of argon cluster bombardment of a copper–graphene film," Fiz. Mezomekh. **17**, 67–73 (2014).
9. A. E. Galashev and V. A. Polukhin, "Compaction of copper film on grapheme by argon-beam bombardment: Computer experiment," J. Surf. Invest. X-ray, Synchr. Neutr. Techn. **8**, 1082–1088 (2014).
10. A. Y. Galashev, "Computer study of the removal of Cu from the graphene surface using Ar clusters," Compt. Mater. Sci. **98**, 123–128 (2015).
11. A. Y. Galashev and O. R. Rakhmanova, "Computer simulation of the bombardment of a copper film on graphene with argon clusters," Chin. Phys. B **24**, 020701 (2015).
12. J. Tersoff, "Empirical interatomic potential for carbon with application to amorphous carbon," Phys. Rev. Lett. **61**, 2879–2882 (1988).
13. E. Burgos, E. Halac, and H. Bonadeo, "A semi-empirical potential for the statics and dynamics of covalent carbon systems," Chem. Phys. Lett. **298**, 273–278 (1998).
14. S. J. Stuart, A. V. Tutein, and J. A. Harrison, "A reactive potential for hydrocarbons with intermolecular interactions," J. Chem. Phys. **112**, 6472–6486 (2000).
15. A. E. Galashev and V. A. Polukhin, "Computer study of the physical properties of a copper film on a heated graphene surface," Phys. Solid State **55**, 1733–1738 (2013).
16. A. E. Galashev and S. Yu. Dubovik, "Molecular dynamics simulation of compression of single-layer graphene," Phys. Solid State **55**, 1976–1983 (2013).
17. A. Kutana and K. P. Giapis, "Atomistic simulations of electrowetting in carbon nanotubes," Nano Lett. **6**, 656–661 (2006).
18. P. Schwerdtfeger, P. D. N. Boyd, S. Briennes, J. S. McFearets, M. Dolg, M.-S. Liao, and W. H. E. Schwarz, "The mercury–mercury bond in inorganic and organometallic compounds. A theoretical study," Inorg. Chim. Acta **213**, 233–246 (1993).
19. Y. M. Kim and S.-C. Kim, "Adsorption/desorption isotherm of nitrogen in carbon micropores," J. Korean Phys. Soc. **40**, 293–299 (2002).
20. F.-Y. Li and R. S. Berry, "Dynamics of Xe atoms in NaA zeolites and 129Xe chemical shift," J. Phys. Chem. **99**, 2459–2468 (1995).
21. J. F. Ziegler, J. P. Biersack, and U. Littmark, *Stopping and Ranges of Ions in Matter* (Pergamon, New York, 1985), Vol. 1.
22. A. Delcorte and B. J. Garrison, "High yield events of molecule emission induced by keV particle bombardment," J. Phys. Chem. B. **104**, 6785–6800 (2000).
23. F. D. Lamari and D. Levesque, "Hydrogen adsorption on functionalized grapheme," Carbon **49**, 5196–5200 (2011).
24. J. Wilcox, E. Sasmaz, and A. Kirchofer, "Heterogeneous mercury reaction chemistry on activated carbon," J. Air Waste Manag. Assoc. **61**, 418–426 (2011).
25. L. Verlet, "Computer 'experiments' on classical fluids. I. Thermodynamical properties of Lennard-Jones molecules," Phys. Rev. **159**, 98–103 (1967).
26. H. J. C. Berendsen, J. P. M. Postma, W. F. van Gunsteren, A. DiNola, and J. R. Haak, "Molecular dynamics with coupling to an external bath," J. Chem. Phys. **81**, 3684–3690 (1984).
27. B. Hafskjold and T. Ikeshoji, "Microscopic pressure tensor for hard-sphere fluids," Phys. Rev. E: Stat., Nonlin., Soft Matter Phys. **66**, 011203 (2002).
28. A. E. Galashev and O. R. Rakhmanova, "Mechanical and thermal stability of graphene and graphene-based materials," Phys.-Usp. **57**, 970–989 (2014).
29. S. Yu. Davydov, "Energy of substitution of atoms in the epitaxial graphene–buffer layer–SiC substrate system," Phys. Solid State **54**, 875–882 (2012).
30. A. E. Galashev and A. A. Galasheva, "Computer Simulation of Cluster Bombardment of a Lead Film on Graphene," High-Energy Chem. **49**, 117–121 (2015).
31. L. J. Munro and J. K. Johnson, "An interatomic potential for mercury dimer," J. Chem. Phys. **114**, 5545–5551 (2001).
32. M.-C. Duval and B. Soep, "Potential characteristics of the mercury–methane van der Waals complex," Chem. Phys. Lett. **141**, 225–231 (1987).

Translated by S. Gorin